

Effect of heat treating process on phase transformation and photocatalytic activity of Zn-doped nano-titania

Tana Bao^{1,2} ✉, Xiao Tian^{1,2}, Gerile Naren^{1,2}, Tegus Ojiyed^{1,2}

¹College of Physics and Electronic Information, Inner Mongolia Normal University, Hohhot 010022, People's Republic of China

²Inner Mongolia Key Laboratory for Physics and Chemistry of Functional Materials, Inner Mongolia Normal University, Hohhot 010022, People's Republic of China

✉ E-mail: tanaph@imnu.edu.cn

Published in Micro & Nano Letters; Received on 22nd November 2019; Revised on 26th July 2020; Accepted on 21st August 2020

The undoped titanium dioxide (TiO₂) and zinc-doped TiO₂ gels were prepared by sol–gel method. The nano-TiO₂ powders were prepared by controlling the sintering temperature. The phase compositions of the sintered samples were analysed by powder X-ray diffraction; the microstructure was analysed by high-resolution transmission electron microscope; the photocatalytic activity was analysed by photochemical reactions instrument. The combined action of Zn²⁺ doping and heat treatment on phase transformation and photocatalytic performance of TiO₂ were analysed. The results show that, when the Zn ion doping amount is within 1–5 mol%, it promotes the conversion of anatase to rutile transition as the presence of ZnTiO₃. The photocatalytic performance of TiO₂ sintered at 700°C is better than sintered at 400°C.

1. Introduction: Catalyst science has made a very important contribution in the 21st century. The discovery of photocatalytic process has become one of the most promising new technologies for the decomposition of different types of pollutants. The photocatalyst can decompose the stable organic matter under normal temperature and pressure by using sunlight. The nano-sized titanium dioxide (TiO₂) particle photocatalyst with diameter ranging from 1 to 100 nm, which came out at the end of 1980s, is one of the most ideal photocatalyst. It has the characteristics of non-toxicity, odourless, non-irritation, good heat resistance, non-decomposition, non-volatilisation, easy source and so on. It has very broad application prospects [1, 2]. TiO₂ can modify carbon nanotube to prepare composite materials (TiO₂/CNT) by chemical deposition [3] and the TiO₂ nano-powder can even be made into TiO₂ nanotubes [4].

As a photocatalyst, TiO₂ has many advantages, but it also has some disadvantages. TiO₂ has a wide bandgap (e.g. the bandgap of anatase is $E_g = 3.2$ eV, and the bandgap of rutile is $E_g = 3.0$ eV). The photocatalytic activity of TiO₂ can only be stimulated in the ultraviolet range. The ultraviolet wavelength is <400 nm, accounting for 5% of the total solar energy, and the visible light wavelength is concentrated at 400–760 nm, accounting for 45% of the total solar energy [5, 6]. Therefore, the photocatalytic activity of TiO₂ is almost ineffective in the visible light range, which greatly limits its photocatalytic application under visible light irradiation. In recent years, researchers have done a lot of research and have found that the photocatalytic efficiency can be improved by inhibiting the combination of photogenerated electrons and holes [7]. In order to improve the photocatalytic performance of TiO₂, many methods have been used to modify it, including metal ion and non-metal ion doping [8, 9], heat treatment [10] and surface modification [11]. Among them, metal ion doping is the most effective way to improve the photocatalytic performance of TiO₂ and broaden its spectral response range. When doped metal ions are deposited on the surface of TiO₂, the combination of photogenerated electrons and holes are effectively suppressed, thus improving the efficiency of photocatalysts. Therefore, the crystal structure of TiO₂ can be optimised by doping appropriate amount of metal ions to improve its physicochemical properties and photocatalytic properties [12–14]. Transition metal ion doping is an important research direction of TiO₂ doping modification. Since the transition

metal ions can change the crystal morphology and energy level structure of nano-TiO₂ after doping, impurity levels can be formed and photons with smaller energy can also be transitioned. This thus causes its absorption of light to red-shifted, expanding its absorption wavelength range, and improving the utilisation of visible light [15].

Researchers have done more studies on zinc-doped TiO₂ which were prepared by different methods. Fu *et al.* [16] have reported that the doping of zinc could induce a significant change of particle size, then affecting the photoelectric properties. Mei Yang *et al.* [17] prepared the zinc-doped micro-arc oxidation (MAO)-TiO₂ films using titanium substrate and Zn(NO₃)₂ solution. They discovered that Zn doping broadens the absorption spectra of the investigated films and the excitation wavelength of MAO Zn film electrode was extended to the visible light range. Recently, the Zn-, N- and S-doped TiO₂ films were prepared by sol–gel method and their photocatalytic degradation was analysed. The results showed that the TiO₂/Zn-urea thin films with the highest efficiency decomposition are recycled and permanent, showing a good potential of this technique in practical application [18]. At the same time, the Zn-doped TiO₂ thin film was synthesised by a thermal spray pyrolysis technique with an aim to investigate the influence of Zn doping on the structural, morphological, optical and the electrical properties of TiO₂ nanoparticles. The results indicate that the crystallite size and the lattice strain evaluated are highly intercorrelated [19].

In this Letter, the undoped TiO₂ and Zn²⁺-doped TiO₂ gel were prepared by sol–gel method and then sintered at different temperatures. The phase transformation process was analysed by X-ray diffractometer (XRD) and high-resolution transmission electron microscope (HRTEM). The photocatalytic performance was tested by the photochemical reactions instrument. Finally, the effects of Zn²⁺ ion doping and heat treatment on the phase transformation, microstructure and photocatalytic performance of TiO₂ were discussed.

2. Experimental

2.1. Sample preparation: The titania sol was prepared by sol–gel method using analytical reagents (AR) tetrabutyl titanate (Beijing Chemical Reagent Co. Ltd.) as precursor and AR grade absolute

alcohol (Sinopharm Group) as solvent. For the Zn^{2+} -doped titania, the AR grade $\text{Zn}(\text{NO}_3)_2 \cdot 6\text{H}_2\text{O}$ (Tianjin Kaitong Chemical Reagent Co. Ltd.) was dissolved into absolute ethanol according to the ratio of 1, 5, 25 mol% zinc ion and then dipped into the tetrabutyl titanate and stirred vigorously. The TiO_2 gel was obtained by dropping 36 vol.% acetic acid (Tianjin Fengchuan Chemical Reagent Technology Co. Ltd.) and then the gel was dried at 80°C . Finally, the xerogels were annealed at 400, 600 and 700°C for 2 h and the powders were fully grinded to obtain powder with particle size 74–63 μm (ASTM E11-58T).

2.2. Sample characterisation: The phase composition of the samples was analysed by XRD (D/MAX-2500/PC, PIGAKV), using copper Ka radiation and the scanning ranged from 2θ of 20° to 80° .

The morphology, interplanar spacing and orientation of the TiO_2 were characterised using HRTEM (JEM-2010, JEOL) with a point resolution of 0.23 nm, lattice resolution of 0.14 nm. The TiO_2 powders were dispersed by absolute alcohol and dropped on a carbon film supported by a copper grid.

2.3. Photocatalytic test: The XPA-7 multi-tube stirring reactor was used to test the photocatalytic performance of TiO_2 . The instrument mainly consists of quartz cold trap, light source, filter, glass tank and tube rack, disk, motor controller and so on.

The effect of samples on degradation rate of methylene blue (with purity of 98.5%, Tianjin Fengchuan Chemical Reagent Technology Co. Ltd.) was tested. First, 0.0015 g methylene blue was weighed and put into 200 ml secondary distilled water to prepare simulated pollutant methylene blue solution. Every 0.05 g of TiO_2 photocatalyst (doped with Zn or pure TiO_2) with different content and sintering process was added in the test tube, respectively, and then 10 ml methylene blue was added as the blue aqueous solution of the pollutant. Three copies of each sample were prepared for testing.

Then the prepared mixture was put into a XPA-7 multi-tube stirring reactor for 30 min for dark reaction, and a magnetic stirrer was used to achieve adsorption–desorption balance. After the dark reaction for 30 min was completed, the photocatalytic reaction was conducted under the irradiation of ultraviolet, and the reaction lasted 60 min. During the reaction, samples were taken every 20 min and centrifuged three times through a centrifuge at high speed. Then the supernatant was taken and its absorbance was measured with a visible light spectrophotometer (722, Shanghai Youke Instrument Co. Ltd). In order to reduce the error, three test tubes were prepared for each group of samples and the absorbance was measured for three times. Finally, the average value was taken.

Finally, the photocatalytic degradation rate of methylene blue (η) was calculated by using the measured absorbance formula [8]

$$\eta = (A_0 - A_1)/A_0 \times 100\% \quad (1)$$

A_0 and A_1 are the absorbance of solution before and after degradation.

3. Results and discussion

3.1. XRD analysis: Different sintering temperatures also affect the crystallisation and phase transformation of TiO_2 . Studies have shown that when the sintering temperature is as low as 200°C , small amount of anatase crystals were observed in the amorphous gel [20].

Fig. 1a shows the XRD pattern of TiO_2 powders sintered at 400°C for 2 h. It can be seen in the figure that the main phase of undoped TiO_2 and Zn-doped TiO_2 samples sintered at 400°C were anatase (A). The diffraction peaks of all samples are wider and the intensity is weaker compared to the sample sintered at 600 and 700°C . It indicates that the anatase particles are very fine and the crystallisation is incomplete. On the other hand, the intensity of diffraction peaks of 1

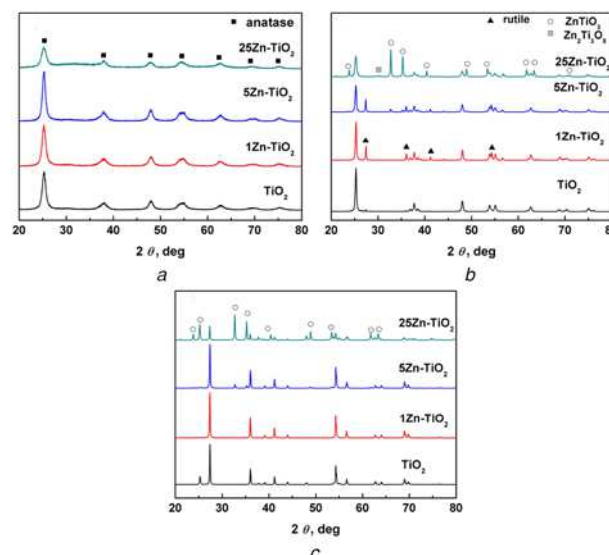


Fig. 1 XRD pattern of TiO_2 sintered at
a 400°C
b 600°C
c 700°C , for 2 h

and 5 mol% Zn-doped TiO_2 is stronger than that of undoped TiO_2 , while the diffraction peak of 25 mol% Zn-doped TiO_2 is the weakest. It can be seen that as the amount of Zn-doping increases, the crystallisation of TiO_2 is first promoted and then inhibited. Initial stage, Zn^{2+} ion doping promotes the conversion of gel to anatase, which is considered to be that ion doping makes the amorphous network structure of TiO_2 no longer stable, leading to an increase in the free energy of the system, which is beneficial to the crystallisation of the amorphous structure.

In Fig. 1b, when the temperature is raised to 600°C , for the undoped TiO_2 , sharp anatase diffraction peak occurred, and for the 1 mol% Zn-doped TiO_2 , the anatase was began to convert into rutile (R). The main phase of 5 mol% Zn-doped TiO_2 is anatase, and ZnTiO_3 is detected in addition to rutile. With the increase of ion doping, ZnTiO_3 began to dominate in 25 mol% Zn-doped TiO_2 , and contained some anatase, and no rutile was detected. The results show that, when the Zn^{2+} ion doping amount is within 1–5 mol%, it promotes the conversion of anatase to rutile transition as sintered at 600°C . Studies have shown that ZnTiO_3 and rutile have similar dense packing structures and their Ti–O bond lengths are similar as well. Therefore, the presence of ZnTiO_3 is equivalent to the addition of rutile seeds, which makes it easier to produce rutile for the 1–5 mol% Zn-doped TiO_2 .

In Fig. 1c, the sintering temperature is further raised to 700°C , the content of anatase in undoped TiO_2 is reduced, and the main phase is converted into sharp rutile. The 1 and 5 mol% Zn-doped TiO_2 are mainly rutile. For the 25 mol% Zn-doped TiO_2 , the ZnTiO_3 is the main phase and includes some rutile. Therefore, for a 1–5 mol% Zn-doped sample, the sintering temperature of 700°C is high enough to obtain 100% rutile.

In Fig. 1, except the ZnTiO_3 and small amount of $\text{Zn}_2\text{Ti}_3\text{O}_8$, no ZnO diffraction peak was found for the Zn-doped TiO_2 , especially at low temperature. The diffraction peak position of TiO_2 did not change. It may because the radius of Zn^{2+} and Ti^{4+} was 0.074 and 0.0605 nm, respectively. So, it was almost impossible for Zn^{2+} ions to enter the TiO_2 lattice. Therefore, one can believe that ZnO is highly dispersed on the surface of nano- TiO_2 or aggregated in the grain boundaries as a form of microcrystals without being detected.

Fig. 2 shows the variation of lattice constants of TiO_2 with increasing of Zn^{2+} content. It can be seen from Fig. 2 that the

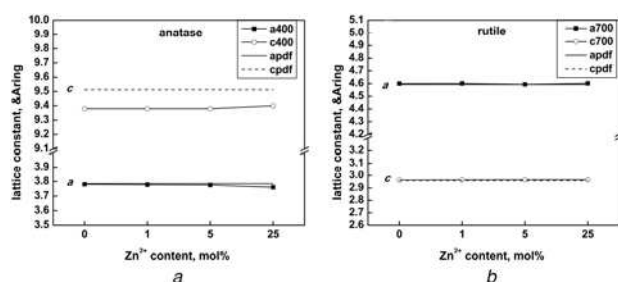


Fig. 2 Variation of lattice constants of TiO_2 crystals with Zn^{2+} content
a Anatase (400°C)
b Rutile (700°C)

lattice constants a and c of the anatase and rutile remain stable. This may be because the Zn^{2+} cannot enter the TiO_2 lattice and cause lattice expansion, so the lattice constant remains basically unchanged. In addition, the anatase lattice constant c at 400°C is lower than the standard value (c pdf in Fig. 2a) because the sintering temperature is low and the crystallisation is not complete. On the contrary, because the sintering temperature is high enough and the crystallisation is complete, the rutile lattice constants a and c at 700°C are close to the standard values (a pdf and c pdf in Fig. 2b).

Therefore, for Zn-doped TiO_2 , the Zn^{2+} ion is failed to enter the TiO_2 crystal lattice, but formed new compounds, such as ZnTiO_3 and $\text{Zn}_2\text{Ti}_3\text{O}_4$ or ZnO , so Zn-doped TiO_2 are actually a composite materials.

Fig. 3 shows the average grain size of undoped and Zn-doped TiO_2 sintered at different temperatures calculated based on the Scherrer equation. It can be seen from Fig. 3a that, when sintering at 700°C, there is no crystal size data of anatase for 1 mol% Zn-doped and 5 mol% Zn-doped TiO_2 . Similarly, when sintering at 600°C, there is no crystal size data of rutile for 25 mol% Zn-doped TiO_2 in Fig. 3b. Both were consistent with the XRD analysis in Fig. 1.

Generally, the grain size of anatase and rutile in both the undoped and Zn-doped TiO_2 increases gradually with the increase of sintering temperature. When sintered at 400°C, the grain size of anatase in all samples was about 10 nm and increased to 45–50 nm when sintered at 700°C.

We have already noticed that with the amount of Zn^{2+} doping increases, the crystallisation of TiO_2 is first promoted and then inhibited at the same sintering temperature. So, the grain sizes of most of the anatase and rutile also vary simultaneously with the increase of Zn-doping. It can be concluded that after the doping amount reaches a certain value, the Zn^{2+} doping effectively inhibits the growth of anatase and rutile. It is also due to its solubility in both the anatase and rutile is far less compared to that in the amorphous TiO_2 . It may be because the Zn^{2+} ions concentrated around the TiO_2

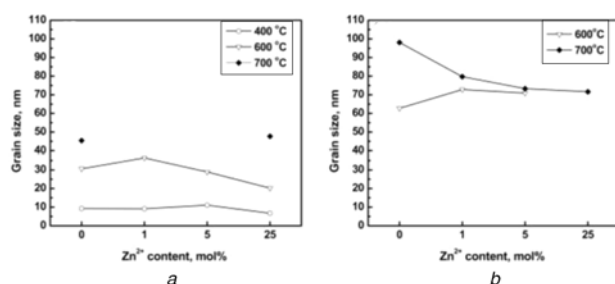


Fig. 3 Variation of crystal size of undoped and Zn-doped TiO_2 with sintering temperature
a Anatase
b Rutile

or form fine oxide particles have dispersing to suppress the diffusion of Ti^{4+} ions into anatase or rutile, and ultimately inhibit the growth of anatase or rutile. The special case is that when sintered at 700°C, the grain size of rutile is keep falling with the increasing of Zn doping. It is because, the crystallisation is perfect at high temperature, so only the inhibiting effect of Zn^{2+} ions on growth of rutile is shown (Fig. 1b).

In general, as the sintering temperature increases, the anatase transforms into rutile, and the crystal structure tends to be stable. When sintered at 400°C, the grain size of anatase is only about 10 nm. So, the lattice is still incomplete, and may grow completely with the sintering temperature increase. Through the Scherrer equation, we also calculated that the average grain size of ZnTiO_3 reaches 94 nm at 700°C.

3.2. HRTEM analysis: Fig. 4 shows a typical crystalline morphology of undoped TiO_2 nanopowders sintered at different sintering temperatures for 2 h. It can be seen from Fig. 4a that the TiO_2 sintered at 400°C for 2 h has crystallised grains of uniform size. In Fig. 4b, the d -spacing of the most of the grain is measured to be 0.352 nm, the lattice plane indices corresponded to anatase {101}.

In Fig. 4c, apparently, the grain size increases as the sintering temperature increases. In addition, hard agglomeration of the nanopowder occurs at 700°C, resulting in agglomeration of large and small particles and poor dispersion of the nanopowder. Wherein, the large particles correspond to rutile, and the small particles correspond to anatase that has not been completely converted. Fig. 4d is a HRTEM image of rutile, in which the crystals with a d -spacing of $d=0.323$ nm correspond to the {110} characteristic plane of rutile.

Fig. 5a is the TEM images of 25 mol% Zn-doped TiO_2 sintered at 600°C, and Fig. 5b is its HRTEM image. In Fig. 5b, the interplanar spacing of the two crystal grains is $d=0.237$ nm and $d=0.352$ nm, respectively, which corresponds to the {004} crystal plane and the {101} crystal plane of anatase. Moiré fringes also appear at the interface of the two grains. In the Fourier transform diagram of the lower right diagram, the angles of the diffraction spots corresponding to the {101} and {004}

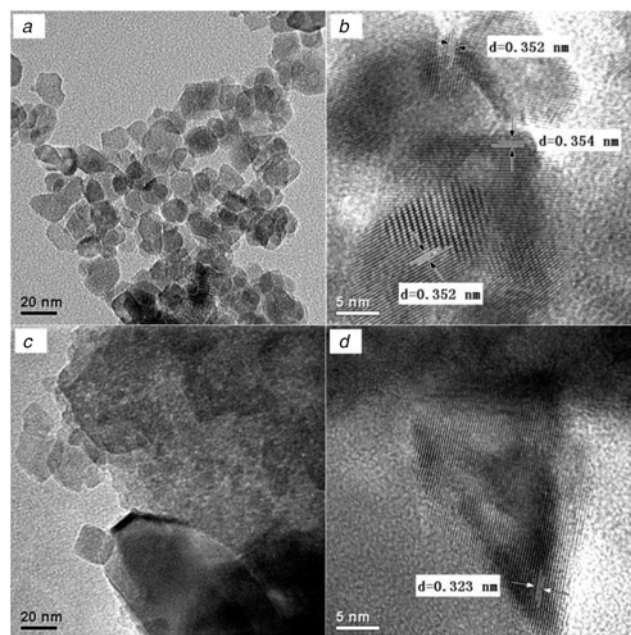


Fig. 4 TEM images of TiO_2 sintered at
a, b 400°C
c, d 700°C

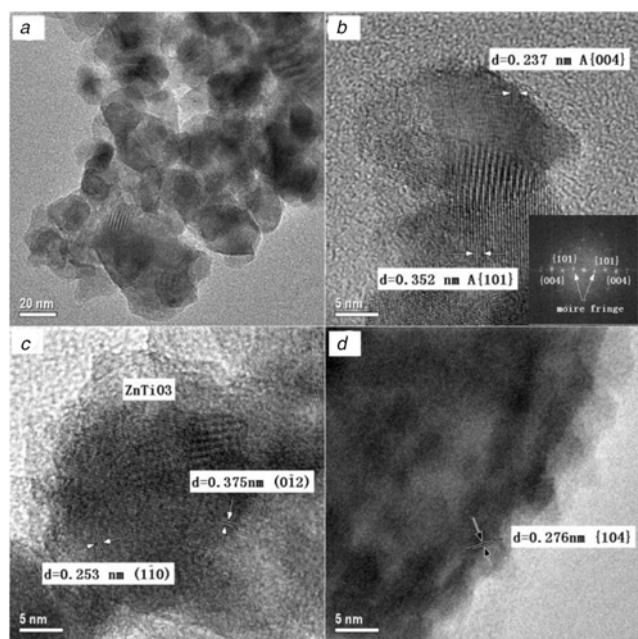


Fig. 5 HRTEM micrographs of 25 mol% Zn²⁺-doped TiO₂ sintered at
a–c 600°C
d 700°C

crystal faces are 2.7°, which is in accordance with the moiré generation condition.

Fig. 5c is the HRTEM image of ZnTiO₃ formed in TiO₂ at 600°C. The *d*-spacing of the two-dimensional crystal faces of the crystal grains is *d*=0.253 and *d*=0.375 nm, respectively, and the angle is about 65.7°, which corresponds to the (110) and (012) faces of ZnTiO₃ observed along the [221] crystal axis (e.g. {110} and {012}; *d*=0.2540 nm, *d*=0.3717 nm, Φ =65.0°; PCPDF No. 26–1500). Fig. 5d is the HRTEM image of ZnTiO₃ formed in TiO₂ at 700°C. The *d*-spacing of the grain is measured to 0.276 nm, the lattice plane indices correspond to ZnTiO₃ {104}. We have directly observed that the ZnTiO₃ grain grows significantly as the sintering temperature increases. The results of TEM are consistent well with those of XRD.

3.3. Effect of Zn doping and heat treatment processes on photocatalytic performance of TiO₂ samples: In the photocatalytic performance test, undoped TiO₂ and 5 mol% Zn-doped TiO₂ were selected from the above samples and studied. As shown in Fig. 6, the degradation rate of organic compounds in all samples increase with the increase of illumination time. In Fig. 6a, the degradation rate of undoped TiO₂ sintered at 400°C is always higher than that of 5 mol% Zn-doped TiO₂. The degradation rate of former is reached 94%, while the latter is only 82% even after

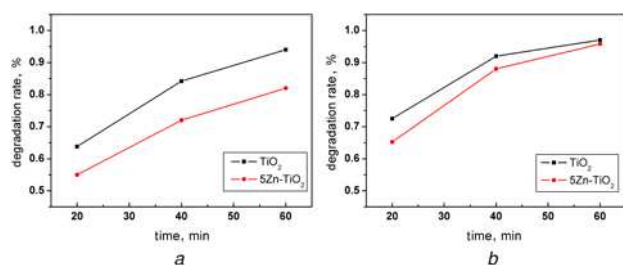


Fig. 6 Degradation rate for MB of specific TiO₂ samples sintered at
a 400°C
b 700°C

60 min. The smaller the grain size of the photocatalyst, the larger the specific surface area, the better the photocatalytic performance. The grain size of undoped TiO₂ sintered at 400°C is smaller than that of 5 mol% Zn-doped TiO₂ (Figs. 1 and 3), which may lead to better photocatalytic performance.

In Fig. 6b, the photocatalytic degradation rates of both samples significantly increase when sintered at 700°C. After 60 min of illumination, the photocatalytic degradation rate of undoped TiO₂ reaches 97%, while the degradation rate of 5 mol% Zn-doped TiO₂ reaches 95.9%. The photocatalytic performance of undoped TiO₂ sintered at 700°C is better than that of 5 mol% Zn-doped TiO₂ because the former contains a certain amount of anatase in addition to rutile, while the latter contains almost no anatase (Fig. 1c) [21].

On the other hand, the photocatalytic performance of TiO₂ sintered at 700°C is better than that of 400°C. This may be due to the incomplete crystallisation of anatase at 400°C, resulting in poor photocatalytic performance (Fig. 1a).

The photocatalytic test suggested that when sintered at 700°C, the satisfying photocatalytic performance appeared for the TiO₂ composed of anatase/rutile. The TiO₂ nanopowder sintered at 700°C was exposed to ultraviolet light for only 60 min, and the degradation rate of MB reached more than 95%, indicating that it has a good application prospect. In addition, it is of great significance to prepare photocatalysts with high degradation rate of organic matter by the economical and simple preparation method of sol–gel method compared to other complex preparing method [17–19].

4. Conclusions: In this Letter, the undoped TiO₂ and 1, 5 and 25 mol% Zn-doped TiO₂ gels were prepared by sol–gel method and then sintered at 400, 600 and 700°C for 2 h. The photocatalytic properties of undoped TiO₂ and 5 mol% Zn-doped TiO₂ were studied by methylene blue solution. The results are as follows.

The main phase of undoped TiO₂, 1 and 5 mol% Zn-doped TiO₂ samples sintered at 700°C was rutile. The diffraction intensity is stronger than that of all samples sintered at 400°C, and the crystallisation is complete. When the Zn ion doping amount is within 1–5 mol%, it promotes the conversion of anatase to rutile transition as sintered at 600°C. The presence of ZnTiO₃ can promote the conversion of anatase to rutile transition.

When sintered at different temperatures of 400 and 700°C, the MB degradation rate of undoped TiO₂ is higher than that of 5 mol% Zn-doped TiO₂. The undoped TiO₂ sintered at 700°C was composed of anatase/rutile and indicates the best photocatalytic performance.

5. Acknowledgments: This work was supported by the Natural Science Foundation of Inner Mongolia (grant no. 2015BS0515); and National Nature Science Fund Project (grant no. 21762033, grant no. 21663018 and grant no. 61804085).

6 References

- [1] Radyum I., Ni L., Nanda H.P., *ET AL.*: ‘Enhanced bone regeneration capability of chitosan sponge coated with TiO₂ nanoparticles’, *Biotechnol. Rep.*, 2019, **24**, pp. 1–8
- [2] Shen J.C., Yang H., Shen Q.H., *ET AL.*: ‘Template-free preparation and properties of mesoporous g-C₃N₄ / TiO₂ nanocomposite photocatalyst’, *Cryst. Eng. Comm.*, 2014, **16**, (10), pp. 1868–1872
- [3] Ye X.Y., Wang Z.P., Wang Q.T., *ET AL.*: ‘Enhanced photocatalytic activity of ternary multilayered Ag / TiO₂ / CNT composites for methylene blue degradation’, *Micro Nano Lett.*, 2019, **14**, (7), pp. 771–776
- [4] Bao T., Ning J., Altan B., *ET AL.*: ‘Microstructure and optical and electrical properties of TiO₂ nanotube thin films prepared by spin-coating method’, *Micro Nano Lett.*, 2019, **14**, (11), pp. 1208–1212
- [5] Fujishima A., Honda K.: ‘Electrochemical photolysis of water at semiconductor electrode’, *Nature*, 1972, **238**, (5358), pp. 37–38

- [6] Asahi R., Morikawa T., Ohwaki T., *ET AL.*: 'Visible light photocatalysis in nitrogen doped titanium oxides', *Science*, 2001, **293**, (5528), pp. 269–271
- [7] Iwasaki M., Hara M., Kawada H., *ET AL.*: 'Cobalt ion-doped TiO₂ photocatalyst response to visible light', *J. Colloid Interface Sci.*, 2000, **224**, (1), pp. 202–204
- [8] Ang Y., He K., Dong Q.X., *ET AL.*: 'Preparation of Zinc doped titanium dioxide and its catalytic degradation of methylene blue', *Rare Met. Mater. Eng.*, 2016, **45**, (1), pp. 360–364 (chinese)
- [9] Wang T., Xu T.: 'Photocatalytic activity of N-doped TiO₂ to vehicle exhaust in road tunnel', *J. Test. Eval.*, 2018, **46**, (3), pp. 1076–1089
- [10] Kumar A., Pandey G.: 'Different methods used for the synthesis of TiO₂ based nanomaterials: a review', *Am. J. Nano Res. Appl.*, 2018, **6**, (1), pp. 1–10
- [11] Liu S.Y., Tang W.H., Yang H.Y., *ET AL.*: 'Regulation of surfactant on microstructure and photocatalytic activity of aluminum doped titanium dioxide powder', *Fine Chem.*, 2013, **30**, (12), pp. 1359–1365 (chinese)
- [12] Chen Z.Y., Fang L., Dong W., *ET AL.*: 'Inverse opal structured Ag / TiO₂ plasmonic photocatalyst prepared by pulsed current deposition and its enhanced visible light photocatalytic activity', *J. Mater. Chem. A*, 2014, **2**, pp. 824–832
- [13] Yi D.J., Chen M.Q., Shi D.J., *ET AL.*: 'Synthesis of porous Ca-doped TiO₂ films and further application in photocatalysis', *Guangzhou Chemical Ind.*, 2018, **46**, (9), pp. 19–22 (chinese)
- [14] Lin H.Q., Tuo X., Ma J.H.: 'Study on degradation of formaldehyde of titanium dioxide composite fabric loaded silver and iron', *J. Funct. Mater.*, 2017, **48**, (3), pp. 3172–3176 (chinese)
- [15] Stucchi M., Boffito D.C., Pargoletti E., *ET AL.*: 'Nano-MnO₂ decoration of TiO₂ microparticles to promote gaseous ethanol visible photoremoval', *Nanomaterials*, 2018, **8**, (9), pp. 686–693
- [16] Fu Y., Cao W., Peng Y.: 'The influence of Zn²⁺ ion doping on the surface morphology and UV photoelectric properties of nano TiO₂ film electrode', *Funct. Mater.*, 2010, **41**, (10), pp. 1780–1783
- [17] Yang M., Huang T.Y., Tang N., *ET AL.*: 'Structure and catalytic performance of Zn-doped TiO₂ film', *Pigm. Resin Technol.*, 2019, **48**, (6), pp. 508–514
- [18] Foulady-Dehaghi R., Behpour M.: 'Visible and solar photodegradation of textile wastewater by multiple doped TiO₂ / Zn nanostructured thin films in fixed bed photoreactor mode', *Inorg. Chem. Commun.*, 2020, **117**. Accepted 15 April 2020, Available online 18 April 2020, doi: 10.1016/j.inoche.2020.107946
- [19] Paul T.C., Podder J.: 'Synthesis and characterization of Zn-incorporated TiO₂ thin films: impact of crystallite size on X-ray line broadening and bandgap tuning', *Appl. Phys. A*, 2019, **125**, pp. 1–14
- [20] Tana Shi Z.M., Chen D.D., *ET AL.*: 'Various analyses of phase transformation from titania gel to anatase crystals', *Rare Met. Mater. Eng.*, 2013, **42**, (11), pp. 2212–2216
- [21] Yu L.Z., Li J.W., Lin Y.H.: 'Progress in photocatalytic properties of transition metal ions doped modified nano-titanium dioxide', *Energy Chem. Ind.*, 2019, **40**, (2), pp. 11–16 (chinese)